Phonon dephasing and population decay dynamics of the G-band of semiconducting single-wall carbon nanotubes

Young Jong Lee,[*] Sapun H. Parekh, Jeffrey A. Fagan, and Marcus T. Cicerone[†]

Polymers Division, National Institute of Standards and Technology, Gaithersburg, Maryland 20899, USA

The dephasing and population decay dynamics of optical phonons are studied for semiconducting single-wall carbon nanotubes (SWCNTs) using broadband time-resolved coherent anti-Stokes Raman scattering and time-resolved incoherent anti-Stokes Raman scattering. By simply adjusting the spectral bandwidth of a continuum pulse, we are able to directly measure both the total dephasing time, T_2, and the population decay time, T_1, of the G-band sequentially in the same sample, which allows for one to exclude artifacts due to comparison of dynamics values measured with different sample conditions and different measurement schemes. The values of T_1 and $T_2/2$ are presented for two different SWCNT samples: bundles in a film on glass and a dispersion in water. While the measured T_1 values are similar for the two samples, the pure dephasing times, $T_2^*/2$, determined from the $T_2/2$ and T_1 measurements are faster in bundled SWCNTs than in isolated dispersion. This suggests that neighboring tubes in the film perturbs the vibrational mode more strongly than surrounding surfactants and that the pure dephasing dynamics is more sensitive to the perturbation.

The unique cylindrical one-dimensional structure of sp^2-bonded carbons makes single-wall carbon nanotubes (SWCNTs) as a group of materials exhibit very interesting electrical, optical, and mechanical properties. Because each specific chirality of SWCNT is a separate species, the exact properties of a given SWCNT population are determined by the distribution of SWCNT structures within a sample. As a nondestructive optical method to characterize SWCNT structure, Raman spectroscopy has been widely used as a primary tool to measure the properties and distribution of nanotube chiralities in a sample by taking advantage of the strong correlation between the structural parameters and the position and shape of Raman bands.[1,2] Compared to most other materials, Raman scattering is greatly enhanced in SWCNTs by a strong electron-phonon coupling, such that one can obtain Raman spectra even from individual SWCNTs.[3,4] Raman spectroscopy has also been used to study the electron-phonon and phonon-phonon interactions, which are critical in various physical phenomena, such as current saturation in high field[5] and superconductivity.[6] Phonon dynamics associated with those phenomena can be studied in both frequency- and time-domain Raman spectroscopies. Line-shape analysis in the frequency domain has been used as a powerful means to study the phonon dynamics associated with the line broadening of spontaneous Raman peaks.[7] However, frequency domain measurements are limited in disentangling various possible line broadening mechanisms, including population decay, pure dephasing, inhomogeneous broadening, and rotational anisotropy decay.

Time-resolved spectroscopy offers a more direct way for identifying and separating the various dynamic processes in the time domain.[8] When an external environment perturbs a vibrational mode, its time evolution in both population and phase can be affected. The time scales of change in the population and the phase indicate the extent of inelastic and elastic perturbations to the vibrational state, respectively. Thus, vibrational dynamics has been extensively studied as a way to understand solute-solvent interactions and solvent dynamics in liquids at various temperature and solvent viscosity.[9,10]

Similarly, phonon dynamics in SWCNT can provide information about intermolecular interactions (e.g., tube-tube, tube-substrate, tube-surfactant, and tube-solvent) and intramolecular interactions (e.g., electron-phonon, phonon-phonon). Time-resolved coherent anti-Stokes Raman scattering (TR-CARS) measures Raman free-induction decay, which is affected by the dephasing and the population decay of generated phonon coherence. Like line-shape analysis in the frequency domain, the Raman free-induction decay is also influenced by other factors, such as inhomogeneous broadening and rotational anisotropy relaxation. Rotational anisotropy relaxation contribution can be easily mitigated in appropriate polarization angle arrangement. However, inhomogeneous broadening contribution is difficult to separate from the Raman free-induction decay. In semiconducting SWCNT, the G-band has been well described with a Lorentzian line shape in Raman spectra[7] (implying small inhomogeneous broadening) and recent improved purification techniques can also reduce potential inhomogeneous broadening due to polydispersity in chirality.

In the Markovian approximation limit, when inhomogeneous broadening is negligible, the decay time constant of the Raman free-induction decay $(T_2/2)$ measured by TR-CARS is expressed as $2/T_2 = 2/T_2^* + 1/T_1$, where T_2^* is the pure dephasing time and T_1 is the population decay time. T_1 is usually longer than T_2^* in the liquid phase; the phonon dynamics are thus described in terms of T_2^* only.[10] However, in case of SWCNT, the previously reported T_1 of the G-band are comparable with the total dephasing time (T_2) inferred from the spontaneous Raman linewidth. Therefore, both T_1 and T_2 need to be measured for understanding the phonon dynamics of SWCNT.

Two major approaches have been used for time-resolved spectroscopy for phonon dynamics studies. (1) *Coherent* approaches for the dephasing dynamics, represented by time resolved coherent anti-Stokes Raman scattering (TR-CARS) (Ref. 9) and Raman echo[11] and (2) *Incoherent* approaches for the population decay dynamics, represented by time-resolved incoherent anti-Stokes Raman scattering (TR-IARS).[12]

One widely used coherent Raman approach is TR-CARS, in which pump and Stokes pulses are simultaneously introduced to generate vibrational coherence and a time-delayed probe pulse induces an anti-Stokes signal.[9] Xie and co-workers[13] measured the Raman free-induction decay by controlling time delay among three collinear, tightly focused femtosecond pulses. However, the experimental setup for the three separate, different-wavelength pulses require an elaborate laser system for wavelength conversion. Later, Kano and Hamaguchi[14] and Lee and Cicerone[15] demonstrated a much simpler way for TR-CARS, which can measure vibrational dephasing times of multiple Raman modes at a single measurement by using one oscillator laser to generate a narrowband pulse and a continuum pulse with a nonlinear optical fiber. Recently, Ikeda and Uosaki[16] measured the dephasing dynamics of optical phonons in a SWCNT film with broadband TR-CARS. However, the temporal resolution was limited to ~1 ps in that experiment.

In TR-IARS, a femtosecond pump pulse creates an electronically excited state, whose energy is incoherently converted to vibrationally excited states or phonons.[12] Subsequently, a delayed probe pulse monitors the anti-Stokes Raman signal from the incoherently prepared phonons. TR-IARS has been widely used to measure optical phonon lifetimes (T_1) of various semiconductor materials.[12,17] Recently, Heinz and co-workers[18] and Kang and co-workers[19] used TR-IARS to measure the optical phonon lifetimes of semiconducting SWCNTs. They found the optical phonon lifetime of the G-band is 1.1 ps for SWCNT suspension and 1.2 ps for SWCNTs deposited on Al_2O_3, respectively. They compared the values of T_1 measured in the time domain with linewidth values measured by other groups in the frequency domain; however, this comparison can be readily influenced by differences in sample condition and purification of SWCNT. A simultaneous or back-to-back measurement of both T_1 and T_2 for the same sample will allow one to avoid potentially misleading analysis occurring by comparing results from different sample conditions.

Here, we demonstrate that we can measure both the total dephasing time, T_2, and the population decay time, T_1, of optical phonons back-to-back at identical sample regions by simple adjustment of the continuum bandwidth with optical filters. Using an optimized continuum generation,[20] we are able to measure the $T_2/2$ and T_1 with an improved temporal resolution for the G-mode phonon of semiconducting SWCNTs. We present the measured dynamics of SWCNTs in a film deposited on a glass coverslip and in a dispersion in water. These consecutive time-resolved Raman measurements at identical sample regions can provide comprehensive and more consistent dynamics analyses of optical phonons in SWCNTs at different molecular environments.

The experimental setup of the time-resolved broadband CARS has been described previously.[15,20] Briefly, as shown in Fig. 1(a), the output (70 fs, centered at 830 nm) of a Ti:S laser oscillator (MaiTai-DeepSee, Spectra-Physics) was split into two parts. One part was introduced into a photonic crystal fiber (Femtowhite, NKT Photonics) to generate a continuum pulse. The continuum pulse spectrum was adjusted with an 850 nm long-pass filter for TR-CARS or with a set of 850 nm long-pass and 900 nm short-pass filters for TR-
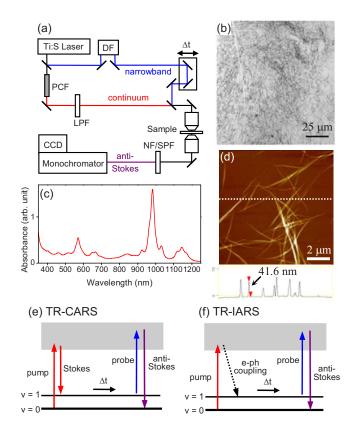

FIG. 1. (Color online) (a) Experimental scheme of the broadband CARS microscopy system used for TR-CARS and TR-IARS measurement: DF, 4-*f* dispersionless filter; PCF, photonic crystal fiber; LPF, long-pass filter; and NF/SPF, notch filter/short-pass filter. (b) Bright-field image of a dried SWCNT film on a glass coverslip. (c) Absorption spectrum of (6, 5) SWCNT dispersion in water with sodium deoxycholate and iodixanol. (d) AFM image of SWCNT bundles in the dried SWCNT film. The line scan of the height at the white dotted line is shown at the bottom. Energy diagrams of (e) TR-CARS and (f) TR-IARS.

IARS. The bandwidth of the remaining oscillator output (the narrowband pulse) was controlled by adjusting slit width in a 4-*f* dispersionless filter to 60 cm^{-1} full-width-half-maximum (FWHM) for optimal temporal resolution when performing TR-CARS and TR-IARS or to ≈5 cm^{-1} FWHM for optimal spectral resolution for spontaneous anti-Stoke Raman scattering. The time delay between the continuum and narrowband pulses was controlled by a stepping motor translational stage (New Focus). The two beams were introduced collinearly and with parallel polarization into a 0.95 NA 40X objective lens (Olympus) and focused on the sample. The CARS signal generated from the sample was passed through a set of an 830 nm notch filter and an 810 nm short-pass filter and was analyzed using a charge-coupled device (CCD) (DU920-BR-DD, Andor) attached to a monochromator (SP-2300, Acton) with a grating of either 300 gr/mm or 1200 gr/mm. To reduce the photoinduced damage of a probed film, the beam was defocused by 4 μm from the surface and the sample was scanned during the CCD exposure time at a speed of >20 μm/s. The excitation power was also reduced so that the signal was not noticeably changed after data acquisition. For measurement in disper-
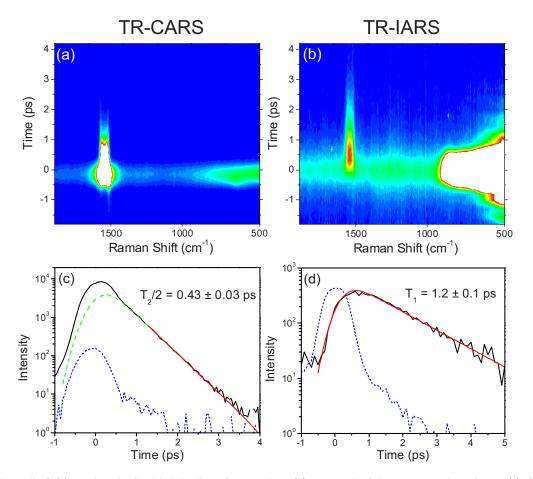
FIG. 2. (Color online) (a) TR-CARS of a dried SWCNT film on glass. (b) TR-IARS of the same sample region as (a). (c) Time profile of the G-band TR-CARS signal averaged between 1570 and 1610 cm^{-1} in (a). The blue dotted line indicates the NRB profile at 1100 cm^{-1}. The green dashed line is calculated for IRF convoluted resonance Raman response using the IRF FWHM of 0.6 ps and the decay time of 0.43 ps. The continuum power is 0.5 mW and the narrowband power is 0.25 mW. The exposure time is 1 s for each time step. (d) Time profile of the G-band TR-IARS signal averaged between 1570 and 1610 cm^{-1} in (b). The blue dotted line indicates the NRB profile at 900 cm^{-1}. The red solid line is calculated using the IRF FWHM of 0.7 ps, the rise time of 0.2 ps, and the decay time of 1.2 ps. The continuum power is 1.1 mW and the narrowband power is 0.25 mW. The exposure time is 10 s for each time step. The uncertainty represents the standard deviation of fitted values from three or more separate measurements.

sion, optical trapping of SWCNTs was avoided by scanning the sample solution repeatedly at a speed of >100 μm/s during the acquisition.

The semiconducting (6, 5) SWCNTs were purified and length-sorted from cobalt-molybdenum catalyst (CoMoCat) nanotubes.[21] The mean length is ≈ 1 μm and the mean diameter is ≈ 0.75 nm. The stock solution was dispersed with 1% by mass per volume sodium deoxycholate as the surfactant; the liquid also contained some iodixanol [(5,5′-[(2- hydroxy-1,3- propanediyl)-bis(acetylamino)]-bis-[N,N′-bis(2,3-dihydroxylpropyl)-2,4,6-triiodo-1,3 -benzene-carboxamide]), purchased as Opti-Prep (Sigma)]. To produce a dried film of SWCNTs the dispersed solution was dropped on a glass coverslip and washed with methanol several times to reduce the amount of surfactant; with this processing the SWCNTs form various sizes of bundles on the substrate from 0.75 to 100 nm in diameter, as shown in the atomic force microscopy (AFM) image of Fig. 1(d).

Figure 2(a) shows TR-CARS spectra of a dried (6, 5) semiconducting SWCNT film on a glass coverslip pumped with a continuum pulse ranging from 840 to 1250 nm. We

obtain a remarkably strong CARS signal at the G-band frequency (≈ 1590 cm^{-1}) considering the low sample density. A significant signal enhancement is expected due to overlap between the broad electronic absorption (E_{11} transition) of these SWCNTs [see the absorption spectrum in Fig. 1(c)] and the energy of the excitation lasers used. The strong optical nonlinearity[22] of SWCNTs also boosts the CARS signal enhancement as demonstrated in four-wave mixing microscopy of individual SWCNTs.[23] The temporal response of the non-resonant background (NRB) signals, shown as the dotted line in Fig. 2(c), corresponds to the instrumental response function (IRF) associated with the cross correlation between the continuum and narrowband pulses. The bandwidth of the narrowband pulse was broadened until the IRF duration is determined by the continuum pulse width.[20,24] The FWHM of the optimized IRF is 0.60 ps with a narrowband pulse of 60 cm^{-1} bandwidth (≈ 200 fs), which is much broader than the typical G-band linewidth of SWCNTs (6–12 cm^{-1}).[7] The decaying CARS signal at the G-mode of 1590 cm^{-1} was fitted only at time delays greater than 1.3 ps to avoid the superposed contribution from NRB interference and two-
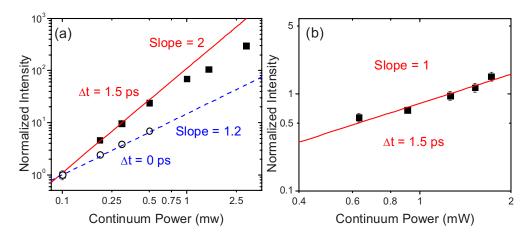
FIG. 3. (Color online) Power dependence of the G-band intensity of (a) TR-CARS and (b) TR-IARS on a dried SWCNT film on glass.

color CARS signal at time zero (the details will be discussed later in this paper). The best fit for the dephasing time constant is $T_2/2 = (0.43 \pm 0.03)$ ps. This value is much shorter than the previously reported value of $T_2/2 = (1.1 \pm 0.1)$ ps.[16] This difference may be due to different SWCNT samples or different film preparation conditions or because the pulse width of the probe pulse (≈ 1 ps in that study) was not sufficiently short to detect the faster dynamics.

Figure 2(b) shows TR-IARS data pumped by a continuum pulse whose wavelength range is narrowed to (840–900 nm) by simply inserting a short-pass filter into the continuum beam path before the two beams are combined. This wavelength range is incapable of populating the G-band phonon either impulsively within the continuum pulse (three-color CARS) or by interacting with the probe pulse (two-color CARS). The TR-IARS signal intensity at 1590 cm^{-1} is reduced by three orders of magnitude compared with the TR-CARS by the broadband continuum excitation at a similar power. The very strong signal below 1000 cm^{-1} in Fig. 2(b) is from two- and three-color CARS. The excitation continuum photon energy (1.4–1.5 eV) corresponds to the phonon sideband of the E_{11} transition.[25] The weak anti-Stokes Raman signal at 1590 cm^{-1} is generated from an incoherently prepared phonon via electron-phonon coupling from an electron-hole pair prepared by the excitation pulse. Since the TR-IARS signal is unaffected by any coherent interference from nonresonant background, the time profile can be analyzed directly by deconvolution with the IRF. The time evolution is fitted with a two-step kinetics model with a rise time and a decay time. The rise time is fitted to be $\approx (0.2 \pm 0.1)$ ps and the decay time is (1.2 ± 0.1) ps. The fast rise time is consistent with the typical electron-phonon coupling rate of the E_{11} state.[18,19,26] The decay time, corresponding to the phonon lifetime, agrees well with the previous measurements.[18,19]

To verify that we are indeed measuring a coherent phonon dephasing time and an incoherent phonon lifetime, we measure the dependence of the TR-CARS and TR-IARS signals on the continuum power, which should be distinct based on the different signal generation mechanisms. The TR-CARS signal is generated via the three-color CARS mechanism, where the signal is proportional to square of continuum power because two transitions (pump and Stokes) are in-

duced by the continuum pulse [Fig. 3(a)].[24] On the other hand, in Fig. 3(b), the TR-IARS should be linearly proportional to continuum pump power since the monitored phonon population is proportional to the product of the electronic excitation rate by the (continuum) pump and the electron-phonon coupling yield. Figure 3(a) shows TR-CARS intensities measured at $\Delta t = 1.5$ ps as a function of continuum power. The power exponent below 0.5 mW for TR-CARS at $\Delta t = 1.5$ ps in Fig. 3(a) is close to two while the TR-IARS shows linear power dependence in Fig. 3(b). This power dependence confirms that the measured signals in Figs. 2(a) and 2(b) correspond to TR-CARS and TR-IARS signals, respectively.

It is noted that the TR-CARS signal deviates from the slope of two above 1 mW. This quasisaturation behavior can be related with either permanent photodamage or a transient change in nonlinear susceptibility at the highest powers. However, TR-CARS signals do not change before and after the irradiation for data acquisition between 0.1 and 3 mW, indicating that any permanent photodamage is negligible. Transient change in nonlinear susceptibility may be associated with multiple excitons in such a way that exciton-exciton annihilation reduces the yield of coherent phonon generation by competing with the Stokes transition. For example, a continuum pulse of 1 mW average power will have fluence of $\approx 3 \times 10^{13}$ photon/(pulse cm^2) at the sample position for the beam diameter of 24 μm. From the absorption spectrum[18] and the absorption cross section[27] for the E_{22} transition of (6, 5) SWCNT, we estimate the average absorption cross section to be 3×10^{-13} cm^2/μm for the continuum spectral range of 840–1250 nm. At this excitation condition, 0.9 or 2.4 excitons can be generated per pulse depending on the exciton diffusion length of 90 nm (Ref. 28) or 240 nm.[29] We suggest this as a possible contribution to the effect but do not have sufficient data to reach a conclusion.

Figure 4(b) shows a spontaneous anti-Stokes Raman spectrum acquired from the same sample region for the data of Figs. 2 and 3. With the continuum pulse blocked, the sample was excited only by a narrowband pulse whose bandwidth was reduced to ≈ 5 cm^{-1} by adjusting slit width in the dispersionless filter. The spontaneous anti-Stokes Raman spectrum exhibits a few interesting features. The measured anti-Stokes Raman spectrum shows a single dominant peak at the
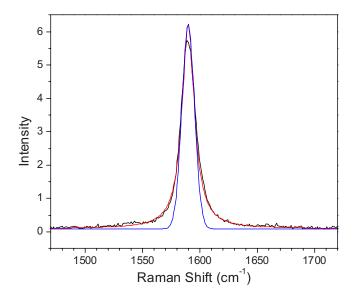
FIG. 4. (Color online) Spontaneous anti-Stokes Raman spectrum of the SWCNT film on glass. The spectrum is obtained with 830 nm excitation (FWHM ≈ 5 cm^{-1}) of 1 mW average power while the sample is scanned at 200 μm/s. The G-band peak fitted with single Lorentzian (red) and Gaussian (blue) functions with FWHM of 13 cm^{-1}. The instrumental resolution for the spontaneous Raman measurements is 5 cm^{-1}.
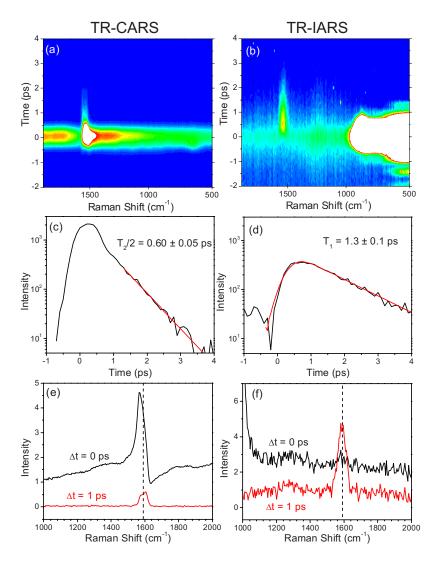
G$^+$-mode resonance frequency at 1590 cm^{-1}. We obtained the better fit to the peak shape with a Lorentzian function than with a Gaussian (see Fig. 4). The Lorentzian line shape and the G$^+$-mode dominant Raman spectrum simplify the linewidth analysis since the resonance frequency of the axial G$^+$-mode is known to be insensitive to diameter and chirality of SWCNTs. The line shape reduces potential contribution of inhomogeneous line broadening due to extrinsic SWCNT properties, such as tube-tube and tube-substrate interactions, tube deformations, and structural defects. The best FWHM fit to the Lorentzian peak is 13 cm^{-1}, which corresponds to 11 cm^{-1} after deconvolving the 5 cm^{-1} instrumental resolution. An 11 cm^{-1} Raman linewidth is consistent with the previously reported linewidth (6–12 cm^{-1}) of isolated SWCNTs on a Si/SiO$_2$ substrate.[7] The Lorentzian line shape and the narrow linewidth strongly suggest that contribution of inhomogeneous line broadening (presumably Gaussian line shape but not necessarily) is very small, compared with homogeneous line broadening. If that is assumed, the pure dephasing time, $T_2^*/2$, can be calculated from the relation, $2/T_2 = 2/T_2^* + 1/T_1$. The calculated $T_2^*/2$ is (0.7 ± 0.1) ps for the semiconducting SWCNT film on glass.

To investigate the influence of molecular environments on phonon dynamics, we measured both the total dephasing time and the population decay time of isolated SWCNTs dispersed in water. These are the same SWCNT solution that was used to prepare the dried film on glass. Figure 5 shows the TR-CARS and TR-IARS data of the surfactant wrapped SWCNTs in solution and the fitted values for the G-band are $T_2/2 = (0.60 \pm 0.1)$ ps and $T_1 = (1.3 \pm 0.1)$ ps. Again assuming inhomogeneous broadening is negligible, the calculated pure dephasing time, $T_2^*/2 = (1.1 \pm 0.1)$ ps. When the measured population decay and pure dephasing times are com-

pared, we find that the population decay time, T_1, is not significantly different between SWCNT bundles on glass and isolated SWCNT dispersion in water beyond the experimental uncertainty. On the other hand, the pure dephasing time, $T_2^*/2$, becomes shorter in the SWCNT bundles on glass than the isolated SWCNT dispersion in water. This suggests that neighboring tubes exert stronger perturbation than surrounding surfactants, which is consistent with the strong tube-tube interaction reported on previous Raman spectroscopy studies.[30,31]

In principle, Fourier transformation of spontaneous Raman line shape in the frequency domain is equal to the corresponding TR-CARS time profile in the time domain. The Lorentzian linewidth of 11 cm^{-1} can be converted to $T_2/2$ of 0.5 ps, which is close to the directly measured value of 0.43 ps in Fig. 2(c). In practice, the two measurements can be complementary to each other. Linewidth analysis will better measure shorter $T_2/2$ ($\sim$broad linewidth); on the other hand TR-CARS will measure longer $T_2/2$ ($\sim$narrow linewidth) with a higher accuracy. The upper limit of measurable $T_2/2$ for linewidth analysis is determined by the spectral convolution of the instrumental resolution and the excitation laser linewidth while the lower limit for TR-CARS is limited by the temporal convolution between the pump and probe pulses (i.e., the instrumental response function). In our frequency- and time-resolved CARS setup, we can use either approach to measure total dephasing times $T_2/2$ depending on linewidth of individual modes.

Now, we discuss the analysis of TR-CARS data around time zero. The TR-CARS signal around time zero contains both two- and three-color CARS contributions[24] and the two- and three-color CARS signals are both interfered by NRB, resulting in dispersive spectral shape, as shown in Fig. 5(c). The CARS signal at time zero is shown to be dominated by two-color generation from the power dependence in Fig. 3(a) (empty circles) where the signal intensity at $\Delta t = 0$ is essentially linearly proportional to the continuum power, as expected for two-color CARS. The extent of spectral shape distortion is not easy to predict because it is nonlinearly affected by various parameters including the ratio of NRB and resonant Raman susceptibilities, the dispersion of the continuum, and the power ratio between the continuum and narrowband pulses. These complicated changes in a CARS spectrum make the TR-CARS time profile [the black solid line in Fig. 2(c)] deviate from that of the resonant susceptibility only at $\Delta t = 0$ ps [the green dashed line in Fig. 2(c)]. Therefore, a simple convolution of the time profile using the IRF is not appropriate to extract the dephasing dynamics parameters. However, as time delay increases, the NRB and two-color CARS contributions die out and only three-color resonant CARS signal survives. The surviving resonant peak is spectrally symmetric, similar to its equivalent spontaneous Raman peak. Therefore, TR-CARS data in this study are fitted later than $\Delta t = 1.3$ ps.

In conclusion, broadband TR-CARS and TR-IARS have been used to measure both of the dephasing time and population decay time of the G-mode in semiconducting (6, 5) carbon SWCNTs. Assuming inhomogeneous broadening is small for the phonon mode, the pure dephasing time has been determined for the G-mode of SWCNT in a dried film on

FIG. 5. (Color online) (a) TR-CARS and (b) TR-IARS of SWCNTs dispersed in an aqueous 1% sodium deoxycholate solution. (c) Time profile of the G-band TR-CARS signal averaged between 1570 and 1610 cm^{-1}. The continuum power is 3 mW and the narrowband power is 2 mW. The exposure time is 2 s for each time step. (d) Time profile of the G-band TR-IARS signal averaged between 1570 and 1610 cm^{-1}. The red solid line shows the best fit with the IRF FWHM of 0.63 ps, the rise time of (0.05 ± 0.05) ps, and the decay time of (1.3 ± 0.1) ps. The continuum power is 2 mW and the narrowband power is 10 mW. The exposure time is 60 s for each time step. (e) CARS and (f) IARS spectra of (a) and (b), respectively, at different time delays.

glass and in a dispersion in water. Dephasing occurs faster in bundled SWCNTs in a film on glass than in the isolated SWCNT dispersion in water, suggesting a stronger interaction with neighboring tubes than with surrounding surfactants.

*yjlee@nist.gov

†cicerone@nist.gov

[1] M. S. Dresselhaus, A. Jorio, M. Hofmann, G. Dresselhaus, and R. Saito, Nano Lett. **10**, 751 (2010).

[2] A. M. Rao, E. Richter, S. Bandow, B. Chase, P. C. Eklund, K. A. Williams, S. Fang, K. R. Subbaswamy, M. Menon, A. Thess, R. E. Smalley, G. Dresselhaus, and M. S. Dresselhaus, Science **275**, 187 (1997).

[3] A. Jorio, R. Saito, J. H. Hafner, C. M. Lieber, M. Hunter, T. McClure, G. Dresselhaus, and M. S. Dresselhaus, Phys. Rev. Lett. **86**, 1118 (2001).

[4] J. C. Meyer, M. Paillet, T. Michel, A. Moreac, A. Neumann, G. S. Duesberg, S. Roth, and J. L. Sauvajol, Phys. Rev. Lett. **95**, 217401 (2005).

[5] J. Y. Park, S. Rosenblatt, Y. Yaish, V. Sazonova, H. Ustunel, S. Braig, T. A. Arias, P. W. Brouwer, and P. L. McEuen, Nano Lett. **4**, 517 (2004).

[6] Z. K. Tang, L. Y. Zhang, N. Wang, X. X. Zhang, G. H. Wen, G. D. Li, J. N. Wang, C. T. Chan, and P. Sheng, Science **292**, 2462 (2001).

[7] A. Jorio, C. Fantini, M. S. S. Dantas, M. A. Pimenta, A. G. Souza Filho, Ge. G. Samsonidze, V. W. Brar, G. Dresselhaus, M. S. Dresselhaus, A. K. Swan, M. S. Ünlü, B. B. Goldberg, and R. Saito, Phys. Rev. B **66**, 115411 (2002).

[8] M. Hase and M. Kitajima, J. Phys.: Condens. Matter **22**, 073201 (2010).

[9] A. Laubereau and W. Kaiser, Rev. Mod. Phys. **50**, 607 (1978).

[10] A. Morresi, L. Mariani, M. R. Distefano, and M. G. Giorgini, J.

Raman Spectrosc. **26**, 179 (1995).

[11] D. Vanden Bout, L. J. Muller, and M. Berg, Phys. Rev. Lett. **67**, 3700 (1991).

[12] D. von der Linde, J. Kuhl, and H. Klingenberg, Phys. Rev. Lett. **44**, 1505 (1980).

[13] A. Volkmer, L. D. Book, and X. S. Xie, Appl. Phys. Lett. **80**, 1505 (2002).

[14] H. Kano and H. Hamaguchi, J. Raman Spectrosc. **37**, 411 (2006).

[15] Y. J. Lee and M. T. Cicerone, Appl. Phys. Lett. **92**, 041108 (2008).

[16] K. Ikeda and K. Uosaki, Nano Lett. **9**, 1378 (2009).

[17] K. T. Tsen, J. G. Kiang, D. K. Ferry, and H. Morkoc, Appl. Phys. Lett. **89**, 112111 (2006).

[18] D. H. Song, F. Wang, G. Dukovic, M. Zheng, E. D. Semke, L. E. Brus, and T. F. Heinz, Phys. Rev. Lett. **100**, 225503 (2008).

[19] K. Kang, T. Ozel, D. G. Cahill, and M. Shim, Nano Lett. **8**, 4642 (2008).

[20] Y. J. Lee, S. H. Parekh, Y. H. Kim, and M. T. Cicerone, Opt. Express **18**, 4371 (2010).

[21] J. A. Fagan, M. L. Becker, J. Chun, and E. K. Hobbie, Adv. Mater. **20**, 1609 (2008).

[22] X. C. Liu, J. Si, B. Chang, G. Xu, Q. Yang, Z. Pan, S. Xie, P. Ye, J. Fan, and M. Wan, Appl. Phys. Lett. **74**, 164 (1999).

[23] H. Kim, T. Sheps, P. G. Collins, and E. O. Potma, Nano Lett. **9**, 2991 (2009).

[24] Y. J. Lee, Y. Liu, and M. T. Cicerone, Opt. Lett. **32**, 3370 (2007).

[25] F. Plentz, H. B. Ribeiro, A. Jorio, M. S. Strano, and M. A. Pimenta, Phys. Rev. Lett. **95**, 247401 (2005).

[26] C. Manzoni, A. Gambetta, E. Menna, M. Meneghetti, G. Lanzani, and G. Cerullo, Phys. Rev. Lett. **94**, 207401 (2005).

[27] S. Berciaud, L. Cognet, and B. Lounis, Phys. Rev. Lett. **101**, 077402 (2008).

[28] L. Cognet, D. A. Tsyboulski, J. D. R. Rocha, C. D. Doyle, J. M. Tour, and R. B. Weisman, Science **316**, 1465 (2007).

[29] A. J. Siitonen, D. A. Tsyboulski, S. M. Bachilo, and R. B. Weisman, Nano Lett. **10**, 1595 (2010).

[30] M. J. O'Connell, S. Sivaram, and S. K. Doorn, Phys. Rev. B **69**, 235415 (2004).

[31] L. Henrard, E. Hernandez, P. Bernier, and A. Rubio, Phys. Rev. B **60**, R8521 (1999).